2006

Cell and Fibronectin Dynamics During Branching Morphogenesis

Melinda Larsen
University at Albany, State University of New York, mlarsen@albany.edu

Cell and fibronectin dynamics during branching morphogenesis

Melinda Larsen, Cindy Wei and Kenneth M. Yamada*

Craniofacial Developmental Biology and Regeneration Branch, National Institute of Dental and Craniofacial Research, National Institutes of Health, 30 Convent Drive, MSC 4370, Bethesda, MD 20892-4370, USA

*Author for correspondence (e-mail: kenneth.yamada@nih.gov)

Accepted 5 June 2006
Journal of Cell Science 119, 3376-3384 Published by The Company of Biologists 2006
doi:10.1242/jcs.03079

Summary

Branching morphogenesis is a dynamic developmental process shared by many organs, but the mechanisms that reorganize cells during branching morphogenesis are not well understood. We hypothesized that extensive cell rearrangements are involved, and investigated cell migration using two-color confocal time-lapse microscopy to image cell and extracellular-matrix dynamics in developing salivary glands. We labeled submandibular salivary gland (SMG) epithelial cells with green fluorescent protein and matrix with fluorescent fibronectin. Surprisingly, we observed substantial, rapid and relatively random migration of individual epithelial cells during branching morphogenesis. We predicted that cell migration would decrease after formation of acini and, indeed, found that rapid cell movements do not occur in SMG from newborn mice. However, in embryonic SMG epithelial cells, we observed an absence of choreographed cell migration, indicating that patterned cell migration alone cannot explain the highly ordered process of branching morphogenesis. We therefore hypothesized a role for directional fibronection assembly in branching. Washout and pulse-chase experiments revealed that older fibronectin accumulates at the base of the clefts and translocates inwards as a wedge, with newer fibronectin assembling behind it. These findings identify a new mechanism for branching morphogenesis involving directional fibronectin translocation superimposed on individual cell dynamics.

Supplementary material available online at
http://jcs.biologists.org/cgi/content/full/119/16/3376/DC1

Key words: Branching morphogenesis, Migration, Salivary gland, Fibronectin

Introduction

Branching morphogenesis is a fundamental process required for the development of many vertebrate organs, including the lung, kidney, prostate, mammary gland and salivary gland, creating a large surface area within the boundary of an organ. The mouse submandibular salivary gland (SMG) has long been used as a model system for the study of branching morphogenesis (Grobstein, 1953). It can be excised from the embryo on the 12th or 13th day of embryonic development (E12 or E13) and grown as an organ explant in culture, where it recapitulates the early stages of in vivo branching. Similar to other organs, branching morphogenesis of the SMG can be divided into a series of steps (Affolter et al., 2003). Branching initiates from a primary bud at E12. Deep 3D indentations – or clefts – form in the surface of the primary bud to subdivide it into separate buds, which is followed by proliferative bud outgrowth. Alternating cleft formation and bud outgrowth continue throughout development to create the multilobular structure of the adult secretory organ. At E13 and earlier, the SMG comprises a solid, nonluminized mass of cells. By E16, the buds have formed early acini, secretory units consisting of a single-cell layer surrounding a central lumen, which are connected by hollow ducts.

It is clear that to create a highly ordered, ramified structure from a simple primary bud, cell rearrangements must occur; however, the nature of the cell behaviors required, and how these behaviors are coordinated in space and time, have not been identified. The related process of tubulogenesis is better understood based on studies of 3D cell culture model systems (O'Brien et al., 2002), which were first developed using mammary gland cells (Barcellos-Hoff et al., 1989). Studies of Madin-Darby canine kidney (MDCK) cells, which form spherical monolayers surrounding a central lumen, or cysts, when embedded in a collagen type I matrix, led to a model for tubulogenesis in which cell migration (Ridley et al., 2003) is the first step (Pollack et al., 1998). Whether cell migration, without disrupting tissue architecture, is also involved in branching morphogenesis is unclear.

Previous studies identified the extracellular matrix protein fibronectin (FN) as an epithelial product that is assembled into the basement membrane and is crucial for branching morphogenesis (Sakai et al., 2003). Knockdown of FN function by inhibitory antibodies or siRNA prevented branching morphogenesis, whereas exogenously added FN stimulated branching morphogenesis, but other ECM molecules did not. FN is expressed by salivary gland epithelial cells, as shown by in situ hybridization and real-time reverse transcriptase (RT)-PCR analyses of laser-capture microdissected cells, and it is expressed at substantially higher levels in cleft epithelial cells than in end-bud epithelial cells (Sakai et al., 2003). A mechanism for FN involvement in branching morphogenesis was identified in which cell-cell

adhesions dependent on E-cadherin are replaced with FN-containing cell-matrix adhesions in the cleft region; however, it was not clear how this mechanism could propagate a forming cleft.

Although branching morphogenesis is a dynamic process, it has been studied largely using static images to infer a sequence of events. Because the epithelial structure of organ explants containing mesenchyme can be resolved with traditional light-microscopy techniques, time-lapse microscopy has been used recently to document morphological changes in salivary gland organ explants during development (Larsen et al., 2003). Although cell migration has been hypothesized to play a role in branching morphogenesis, it has not actually been directly demonstrated, e.g. by tracking individual cells. We combined the imaging of cell movements by tracking green fluorescent protein (GFP)-labeled cells together with parallel imaging of fluorescently labeled FN to investigate the roles of cell migration and matrix remodeling during branching morphogenesis. Using confocal microscopy, we tracked cell and FN dynamics in three dimensions over time. This study documents and provides insight into the surprisingly dynamic nature of cell-cell and cell-matrix interactions during early development.

Results

We hypothesized that coordinated epithelial cell movements are required to form the highly ordered branched structure of SMGs. We utilized time-lapse microscopy to investigate this possibility. In fact, careful examination of time-lapse images from previous studies (Larsen et al., 2003) (see video at http://wwwdir.nidcr.nih.gov/dirweb/cdbrb/DMD/larsen/DB/movies.asp) suggested the possibility of dynamic movements. We therefore used conventional time-lapse imaging of SMG organ cultures at a resolution where we could discern individual cells to search for epithelial cell moments. We observed dynamic epithelial movements in E13.5 SMGs (see Fig. 1A,B and supplementary material Movie 1). Although it was possible to resolve individual cells, it was difficult to monitor their behavior over time with this method (Fig. 1B).

To label and follow individual cells, we used an adenoviral (Ad) vector (Ad-GFP) to deliver the fluorescent cytoplasmic marker GFP to epithelial cells. Although adenovirus can infect both epithelial and mesenchymal cells, it does not readily penetrate into the epithelium of an intact SMG that contains mesenchyme cells (M.P.H. and M.L., unpublished observation). Ad-GFP was therefore microinjected into an end bud (Fig. 1C,D) of an intact E13.5 SMG and monitored by time-lapse microscopy beginning 24 hours after injection. GFP-labeled cells were clearly motile (supplementary material Movie 2). Ad-GFP did not induce this cell migration, because similar cell movements were observed in an unlabeled, intact SMG (see Fig. 1B and supplementary material Movie 1). Immunostaining of the glands with an antibody recognizing the epithelial marker E-cadherin (Takeichi, 1991) after the time-lapse confirmed that the GFP-expressing cells were epithelial (Fig. 1E).

To improve imaging quality, we examined cell movements in mesenchyme-free rudiments by using confocal time-lapse microscopy. Epithelial SMG rudiments were cultured in a laminin-rich basement-membrane matrix (Matrigel, BD Biosciences) (Kleinman et al., 1986) in the presence of

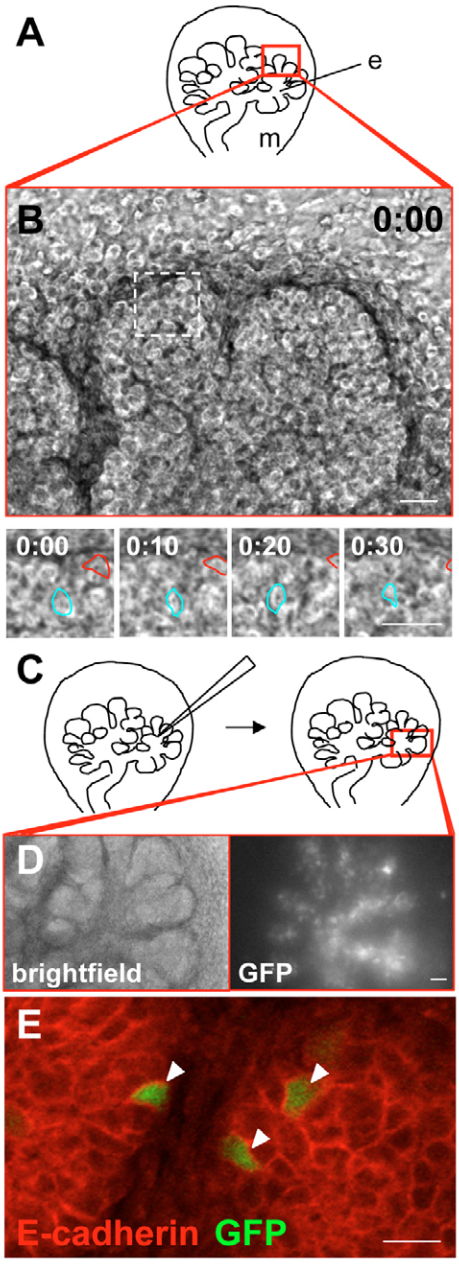

Fig. 1. Epithelial cells in intact salivary glands undergo dynamic movements. (A) Schematic diagram of an intact E13 SMG with epithelium (e) and surrounding mesenchyme (m); the box indicates the region imaged by time-lapse microscopy in panel B. (B) Epithelial buds with surrounding mesenchyme (top) imaged in supplementary material Movie 1 at t=0. The white dashed box indicates the region shown magnified below from individual frames of Movie 1. Two cells that move towards the right are outlined (red and cyan). (C) Schematic diagram indicating the site of Ad-GFP microinjection into epithelium; the box indicates the epithelial region shown in D. (D) First frame from a time-lapse movie showing brightfield-imaged (left) and GFP-labeled cells (right), revealing substantial apparent epithelial cell movements (supplementary material Movie 2). (E) Immunostaining of the microinjected gland after time-lapse analysis with the epithelial marker E-cadherin (red) indicated that the injected GFP-expressing cells (green) are epithelial (arrowheads). Time is indicated in hours:minutes. Bars, 20 μm.

fibroblast growth factor 7 (FGF7) and epidermal growth factor (EGF) (Morita and Nogawa, 1999). Epithelial rudiments incubated in an Ad-GFP-containing solution began expressing GFP in a fraction of the epithelial cells within a few hours after infection. When these epithelial rudiments were analyzed by confocal time-lapse microscopy, remarkably dynamic movements of individual epithelial cells were observed (Fig. 2A,B, supplementary material Movie 3).

To confirm that cells were moving, the distance between individual cells was compared at distinct time-points (Fig. 2C,D). The distance between cells, as measured between the calculated cell centers (centroids), changed over time, indicating that the cells moved relative to each other. In the example shown (Fig. 2), between frames 1 and 2 (elapsed time 24 minutes) the distance between two cells increased by 3.5 μm and in the next 24-minute period by 9.5 μm. In addition, the cells changed shape dramatically over short periods of time (compare shape changes between frames in Fig. 2C).

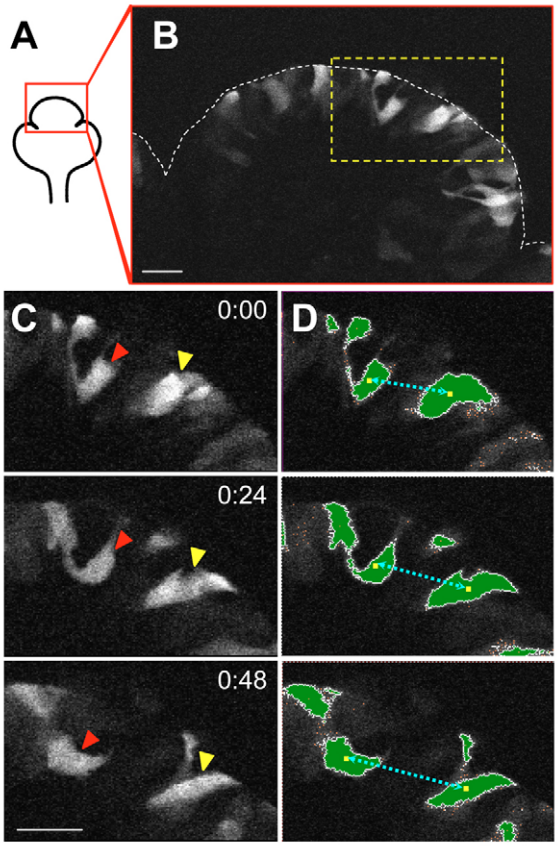

Fig. 2. Mesenchyme-free epithelial cells move relative to each other. (A) Schematic diagram indicating the region of isolated E12 SMG epithelial cells analyzed by time-lapse microscopy in supplementary material Movie 3. (B) First frame of time-lapse Movie 3 with the basement membrane marked by a white dashed line. The yellow dashed box indicates the region examined at higher magnification in C and D. (C) Three frames from time-lapse Movie 3 with cells analyzed in D marked with arrowheads. (D) Frames from C were converted to a binary image (dark green overlay), and cell centroids were calculated automatically (yellow points). The distance between the two cell centroids (cyan dashed line) increased over time, indicating that the cells were migrating: 25.6 μm (0:00), 29.1 μm (0:24), and 38.6 μm (0:48). The velocity varied between frames: 8.7 μm/hour and 23.7 μm/hour. Bars, 20 μm. Time, hours:minutes.

If cell migration is involved in branching morphogenesis, there might be differences in migration rates or patterns in different regions of the gland. As a marker for the epithelial-mesenchymal boundary containing the basement membrane, this zone was labeled with FN. We conjugated purified human plasma FN (Akiyama, 1999; Yamada and Olden, 1978) to the fluorescent label Alexa Fluor-647 (Alexa Fluor-647-FN) and added it to the growth media at a low concentration that does not affect SMG branching morphogenesis (Sakai et al., 2003). Using confocal microscopy, we observed that FN incorporated readily into explants. FN-labeling made it possible to easily distinguish buds from ducts and to identify cells that came into contact with the basement membrane (Fig. 3A, supplementary material Movie 4).

Individual GFP-labeled cells randomly selected from different regions were manually tracked in an SMG undergoing morphogenesis (Fig. 3B). Manual tracking was necessary because of the substantial changes in cell shape between frames. We compared cell tracks of cells located in the interior of buds and in duct regions with bud cells that had contacted the basement membrane. Cell movements were tracked in three dimensions over time, and average cell velocity, displacement and total distance traveled were calculated.

Representative cell tracks are displayed in Fig. 3C as a 3D rose plot in which each cell track initiates from the origin. Although there were substantial variations in behavior between individual cells, cells in different regions tended to migrate with distinctive differences in behavior, which we quantified (Fig. 3C). Epithelial bud cells with diameters of 5.6±1.8 μm moved at a substantial average velocity of 16 μm/hour, equivalent to approximately three cell diameters/hour. The cells traveled meandering paths averaging 80 μm in length over 5 hours tracked. Their net displacement reached up to 45 μm in buds approximately 300 μm in diameter. Bud cells moved more rapidly than duct cells, and the total distance (T) traveled by each bud cell was longer than for duct cells. There was no significant difference in net cell-displacement of bud and duct cells, but bud cells were less processive than duct cells as indicated by their lower meandering index (D/T).

Contact of migrating cells with the basement membrane had significant effects on all aspects of cell behavior. For quantification, cells were included in this category if they touched the basement membrane at any time during the tracking period. On average, cells that contacted the basement membrane moved at a higher velocity, traveled a longer path and showed a greater displacement than bud cells; however, there was no difference in the meandering index.

Since time-lapse movies indicated that the GFP-labeled cells undergo marked changes in shape resembling mesenchymal cell morphology, SMGs were fixed immediately following time-lapse analysis and immunostained with an antibody recognizing the epithelial marker E-cadherin (Fig. 3D). GFP-labeled cells were found interior to the basement membrane demarcated by FN, and all expressed E-cadherin at the cell surface, verifying their epithelial origin. Consistent with time-lapse images showing rapidly shifting cell positions and morphology, individual epithelial cell shapes were highly polymorphic after fixation and staining, as also observed in

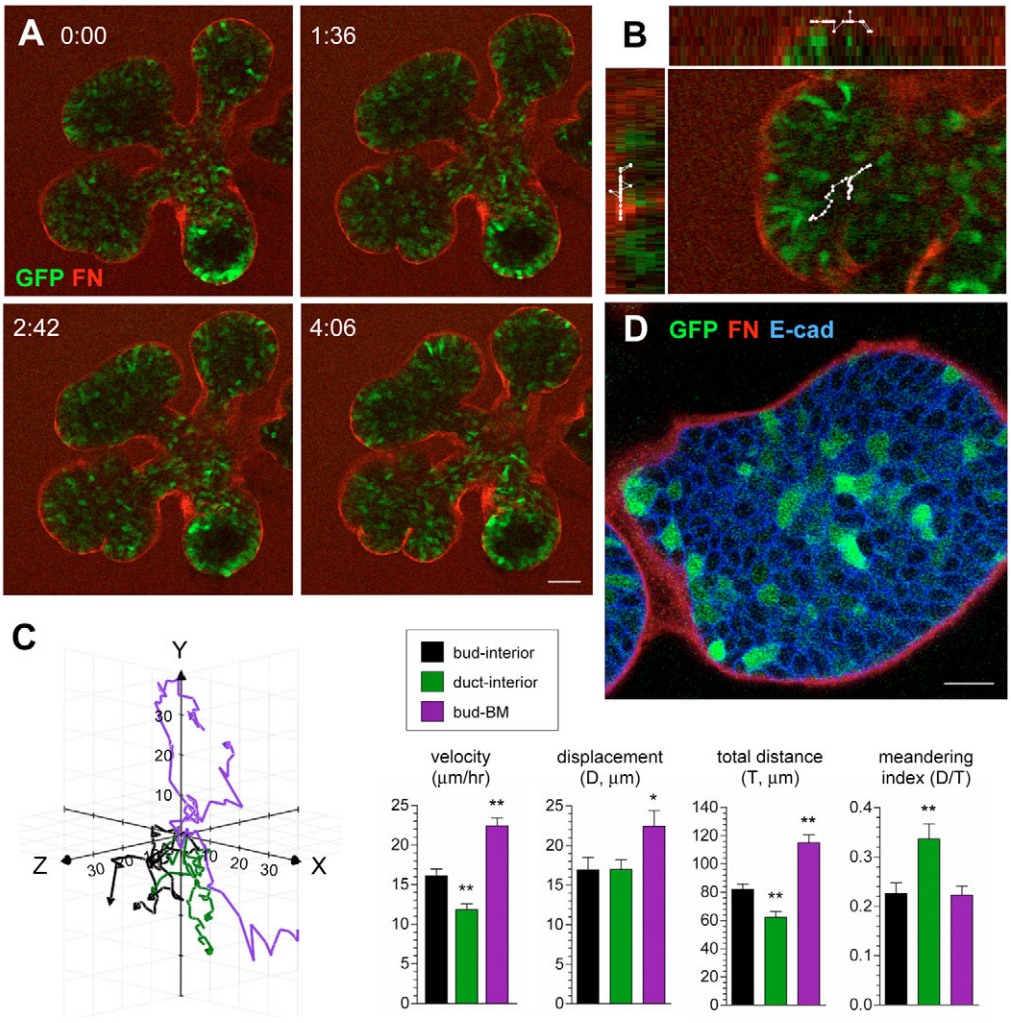

Fig. 3. Epithelial cells show dynamic cell movements that differ in distinct regions of the gland. (A) Still frames from time-lapse supplementary material Movie 4 of E13 SMG epithelia. The frames are single confocal sections through the center of the gland with epithelial cells labeled by GFP (green) and fibronectin labeled with Alexa Fluor-647-FN (red). (B) Individual cell movements were manually tracked in 3D; an example bud track is shown in white overlaid on an *XY* projection with *XZ* (top) and *XY* (left) projections. (C) Representative tracks of migrating cells from the bud interior (black) or duct interior (green) compared to bud cells that had contacted the basement membrane (BM, purple) displayed as a 3D rose plot (*X*, *Y*, and *Z* axis) with the origin of each track at 0, 0, 0. Cell tracks were quantified for velocity (T/*t*), displacement (D), total distance traveled (T), and meandering index (D/T) and displayed as bar graphs: mean ± s.e.m. On average, cells in buds traveled at higher velocities and for longer distances than duct cells, and cells that contacted the basement membrane traveled even faster and further than cells in the interior of buds. Cells were tracked for 5 hours; n=44 (bud), 29 (duct) and 45 (BM), averaged from six experiments. The Wilcoxon signed-rank test was used to calculate statistical significance of differences, *P<0.001, **P<0.0001 compared with bud cells. (D) After time-lapse imaging, the epithelia were fixed and stained with anti-E-cadherin antibody: E-cadherin (blue), GFP (green), and FN (red). All GFP-labeled cells (green) were inside of the basement membrane demarcated by FN, and all expressed E-cadherin. Bars, 50 μm (A), 10 μm (D).

explanted whole glands (Fig. 1E) and glands harvested directly from the embryo (data not shown).

If a unique pattern of cell migration were involved in cleft formation, we hypothesized that cells in the cleft should show a distinct migration pattern compared with other cells, e.g. concerted lateral migration. Instead, no unique migratory characteristics of cells near cleft regions were seen (supplementary material Movie 4 and data not shown). Although some cells located near an advancing cleft moved away, others followed the inward progression of the cleft, and some cells associated only transiently with the cleft and then moved away with variable return to the cleft.

Cells undergoing cell division tend to move away from each other following cytokinesis, and cells in the developing salivary gland proliferate rapidly. Even though cell proliferation itself is not required for cleft formation (Nakanishi et al., 1987), we questioned whether the dramatic cell movements in the developing salivary gland could be merely associated with cell proliferation. Epithelial rudiments were treated with the inhibitor hydroxyurea, which blocks cell division in S-phase of the cell cycle, and then pulse-labeled with the thymidine analog 5-bromodeoxyuridine (BrdU) to detect proliferating cells. BrdU-labeling was substantially inhibited by hydroxyurea (Fig. 4A,B). Epithelial rudiments labeled with GFP and Alexa Fluor-647-FN were treated with hydroxyurea and analyzed by confocal microscopy in comparison with vehicle-treated controls. Cell movements were not reduced by hydroxyurea treatment (Fig. 4B, supplementary material Movie 5) in terms of velocity, total distance traveled or displacement, indicating that cell migration in the developing salivary gland is not merely a result of proliferation.

Our findings suggested that cell migration is a developmentally regulated process involved in forming acinar and ductal structures. If this hypothesis were correct, SMG epithelial cells would be predicted to be motile during early development and to become less motile later after acini have formed. To test this idea, SMGs from day 1 postnatal (P1) mice were labeled with GFP and Alexa Fluor-647-FN, and the epithelia were imaged by confocal time-lapse microscopy

(supplementary material Movie 6). Before initiating tracking, epithelial cells were identified by their location within acini as a circular cluster of cells visible by differential interference contrast (DIC) microscopy surrounded by FN-incorporating cells (mesenchyme); only cells that fulfilled these criteria were tracked (Fig. 5). Cell tracks of P1 epithelial cells revealed little movement (Fig. 5A,B). The velocity, distance traveled and displacement of P1 cells were all minimal compared with E12 epithelial cells (compare Figs 4 and 5, and data not shown), confirming our prediction that SMG cell motility is not needed after acini have formed. In fact, analysis of cells at intermediate developmental stages (E15 and E16) where acini are beginning to form but epithelial cells have not yet formed a monolayer, revealed dynamic movements (data not shown). While these data suggest that cell migration is a component of branching, the lack of a choreographed pattern of cell migration indicates that concerted cell movements alone, such as those in gastrulation, cannot induce the required changes in patterning. Thus, even though the highly plastic nature of the cells might facilitate branching, another component appeared to be required to drive cleft formation.

In previous studies, we had reported that FN is required for branching morphogenesis, because knocking down FN expression or function prevents branching, whereas stimulating SMG with exogenous FN promotes branching (Sakai et al., 2003). However, it was not clear how FN added exogenously to the whole gland could promote local cleft formation, nor how forces required for ingressing cleft formation could be generated by this mechanism. We hypothesized that directional FN assembly creates such a force or external mechanism to

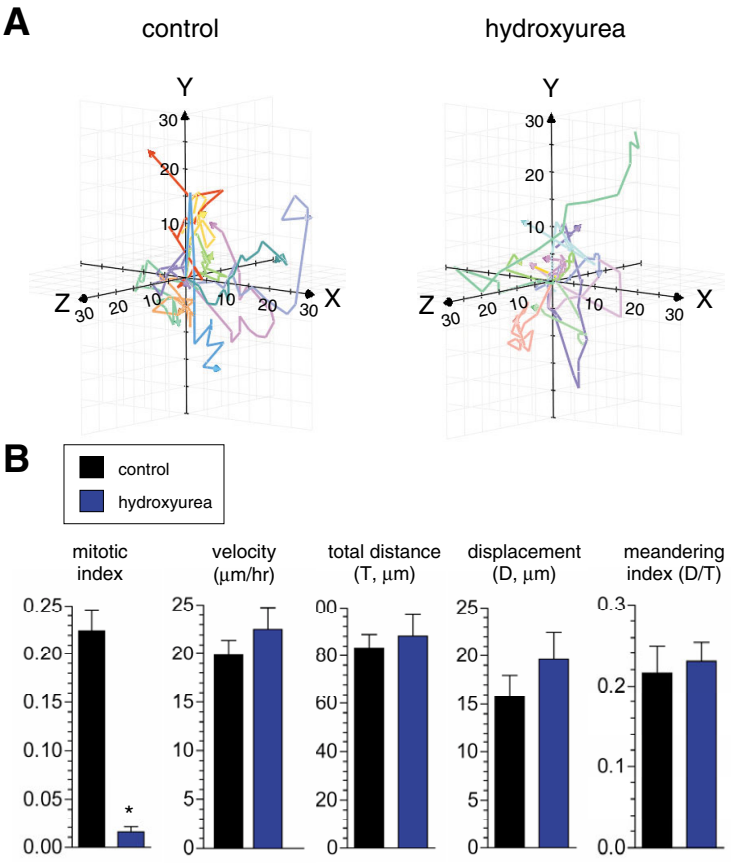

Fig. 4. Cell migration by salivary epithelial cells is not affected by inhibiting cell proliferation. E12 SMG epithelial rudiments were labeled with GFP and Alexa Fluor-647-FN and treated with 0.5 mM hydroxyurea (supplementary material Movie 5). (A) Cells were tracked manually, and 10 representative tracks for each treatment are displayed as 3D rose plots. (B) To measure inhibition of cell proliferation after 24 hours in culture, SMGs were pulse-labeled with BrdU for 3 hours. The mitotic index was calculated as the ratio of total BrdU pixels to total SMG area. Velocity, total distance traveled in 5 hours, displacement and meandering index were calculated as an average of all tracks, and displayed as bar graphs comparing control (black) with hydroxyurea (blue), mean ± s.e.m. Cells were tracked for 3 hours; n=20, averaged from two experiments. Values displayed represent mean ± s.e.m. The Wilcoxon signed-rank test was applied to compare cell tracks of inhibitor-treated SMGs with untreated SMGs, *P<0.05 compared with untreated SMGs.

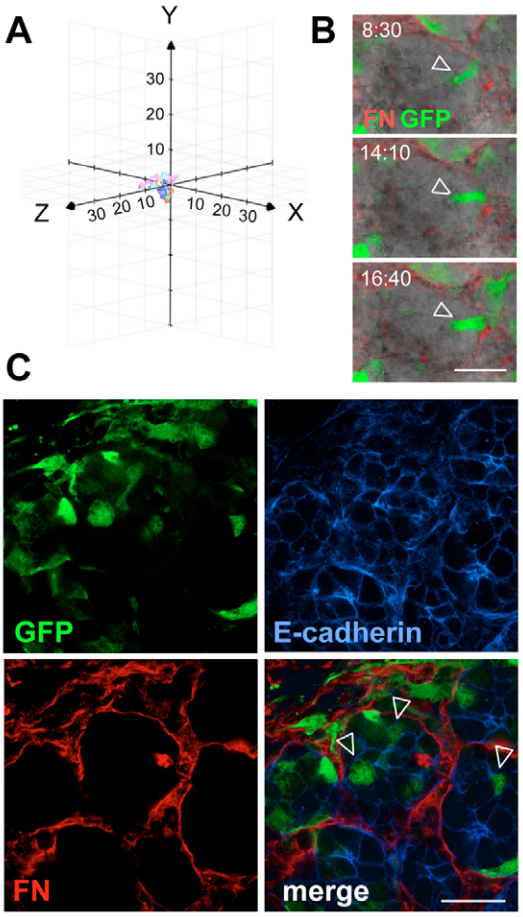

Fig. 5. Cell migration is severely reduced in day 1 postnatal (P1) salivary glands. SMGs from P1 mice were labeled with GFP and Alexa Fluor-647-FN and imaged by confocal microscopy (supplementary material Movie 6). (A) Randomly chosen bud cells were tracked for 5 hours, and migration tracks are displayed as a 3D rose plot, n=10. (B) Frames from Movie 6 showing cells (green) overlaid on a DIC image and surrounded by FN (red). Prior to tracking, epithelial cells were confirmed to be in an acinus surrounded by FN (red). (C) After time-lapse imaging, SMGs were stained with E-cadherin antibody (blue) to reveal epithelial cell boundaries. GFP-labeled cells (green) expressing E-cadherin (blue) were surrounded by FN (red). Bars, 10 μm.

guide cleft formation in the midst of chaotic cell motility. To test for local deposition and directionality of FN assembly, we performed washout and pulse-chase analyses. Epithelial rudiments were labeled with Alexa Fluor-647-FN, and time-lapse imaging was initiated. After approximately 2 hours, the medium was removed and replaced with fresh medium without labeled FN. Imaging of branching morphogenesis following this FN washout revealed that older, labeled FN remained visible as a prominent wedge-shaped aggregate in the deepest part of the cleft (Fig. 6B, supplementary material Movie 7). The rate of FN translocation during cleft propagation was measured from confocal sections and found to be 5.0±1.1 μm/hour. To characterize the dynamics and directionality of FN assembly, Alexa Fluor-488-FN (pseudo-colored green) was incubated with glands for several hours, washed out, and then Alexa Fluor-647-FN (pseudo-colored red) was added to the culture media. Whereas green (older) FN remained intact in the base of the cleft, red (newer) FN accumulated at more distal regions behind the initial cleft in regions lacking the green label. These data indicate that FN is organized and translocated directionally, with newer FN incorporated basally relative to older FN, creating a matrix wedge between the cells as they separate during cleft progression.

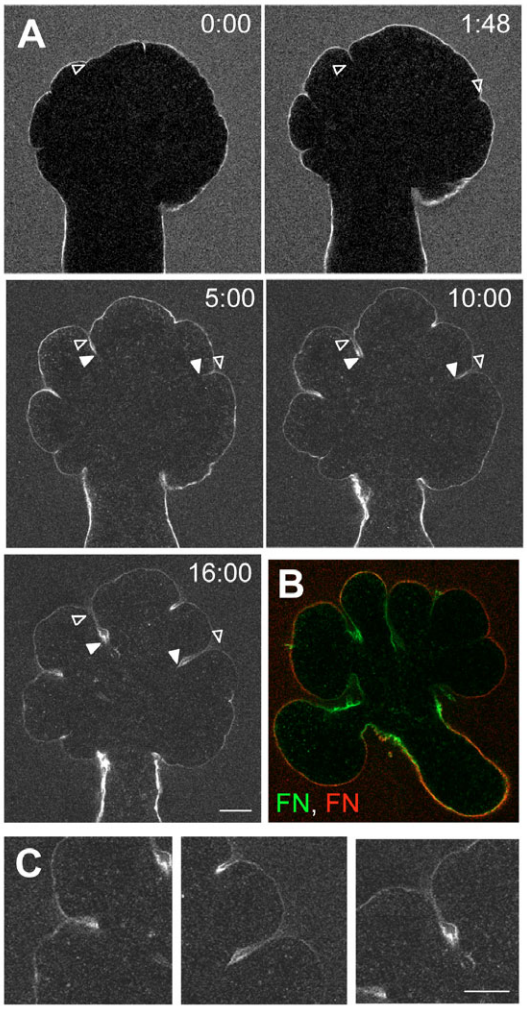

Fig. 6. FN at the base of clefts translocates into the bud whereas newer FN assembles behind older FN. (A) E12 SMGs were labeled with Alexa Fluor-647-FN-containing media for 6 hours and imaged by time-lapse confocal microscopy. After 1 hour 48 minutes of imaging, medium was removed and replaced with fresh medium, and imaging was continued (supplementary material Movie 7). The initiation points of two clefts are labeled with open arrowheads. The bases or bottoms of each of these clefts move inward into the interior of the gland as indicated by filled arrowheads. (B) To image FN displacement, SMGs were incubated with Alexa Fluor-488-FN (green) for 12 hours, washed, and then treated with Alexa Fluor-647-FN (red) for two additional hours. The earliest FN (green) was concentrated at the bottom and lower sides of the cleft, whereas the FN added later (red) assembled in the bud basement membrane and the upper portion of the clefts. (C) Higher-magnification images of clefts at 16 hours from time-lapse images in (A) showing concentration of FN in a wedge-like pattern. Bars, 100 μm.

Discussion

We report here the unexpected finding that individual epithelial cells are highly dynamic and motile in epithelial buds during the developmental process of branching morphogenesis. This finding was unanticipated because epithelial cells are thought to be relatively immobile, except when moving either in small groups (Lecaudey and Gilmour, 2006) or as a cell sheet during developmental- or tissue-repair-processes (Keller, 2002). The dynamic movements we observed were developmentally restricted, because they were not detected in acinar cells of newborn mouse salivary glands. Similar embryonic epithelial cell movements were observed in unperturbed explants and intact explants microinjected with a GFP-expressing adenovirus in the absence of any added growth factors, as well as in intact epithelial rudiments infected with Ad-GFP.

We tracked the movement of individual cells in three dimensions over time within the epithelial rudiments and quantified parameters of cell movement. Tracking and quantification of cell movements has rarely been accomplished in intact mammalian systems, and these studies provide, to our knowledge, the first recordings of epithelial cell movements in developing glands. These cell movements were not a by-product of cell division, because cell migration was unaffected after blocking proliferation with hydroxyurea.

Because the dynamic and apparently non-directed cell movements could not explain the highly ordered process of branching morphogenesis, we compared the concomitant dynamics of fibronectin (FN) during branching as a potential mechanism for inducing branching. Although FN was previously shown to be required for branching morphogenesis (Sakai et al., 2003), the role and mechanics of FN assembly were not clear. We labeled FN fluorescently and examined the dynamics of FN assembly and movement with washout and pulse-chase experiments. FN strongly accumulated at the base of ingressing clefts and translocated into the bud, and new FN assembly occurred behind it.

Based on our findings, we propose a model in which the high degree of cellular dynamics we observe provides sufficient tissue plasticity for regulation by FN; the assembly and translocation of FN towards the gland interior provides a matrix wedge to promote cell separation during cleft progression in branching morphogenesis (Fig. 7).

Specifically, we propose that active FN assembly and integrin-driven lateral translocation into the bud drive cleft formation. FN translocation by fibroblasts was previously

shown to be mediated by α5β1-integrin-containing fibrillar adhesions to generate FN fibrils (Pankov et al., 2000), and the identical integrin is required for SMG branching morphogenesis (Sakai et al., 2003). We show here that FN translocates along SMG epithelial cells into nascent clefts: previously assembled FN ingresses at the base of clefts, whereas newer FN assembles behind it. Exogenously added soluble FN was incorporated specifically into these sites rather than throughout the gland. The rate of FN translocation in SMG epithelial cell clefts was measured here as 5 μm/hour, which is consistent with the 6-7 μm/hour rate of FN assembly and translocation by fibroblasts measured previously (Pankov et al., 2000). We suggest that the translocation of FN deep into the bud replaces cell-cell adhesions with cell-matrix adhesions that promote cleft formation. In fact, we previously reported that FN induced local decreases in cadherin localization in human salivary gland (HSG) cells and that cells adjacent to clefts of developing SMG displayed reduced E-cadherin levels (Sakai et al., 2003).

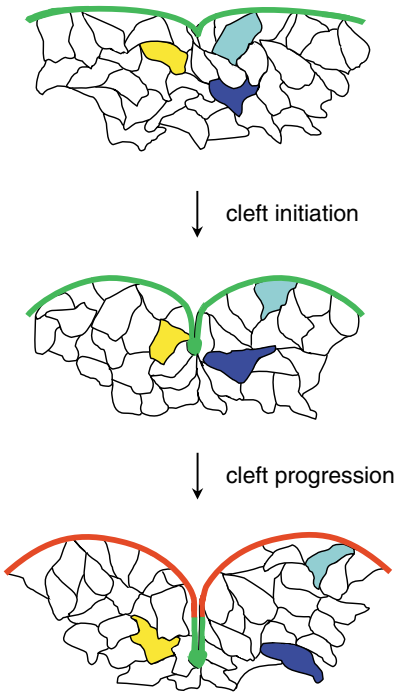

Fig. 7. Working model for roles of cell migration and fibronectin translocation in branching morphogenesis. Cells engage in active migration, providing a highly plastic tissue that is susceptible to local matrix signals. Three representative motile cells have been colored in yellow, blue and cyan. As cleft formation begins, FN is located at the cleft initiation site. Cleft formation proceeds towards the center of the gland with continued synthesis and assembly of FN fibrils by neighboring epithelial cells and dynamic inward progression of an aggregate or wedge of FN between mobile epithelial cells. FN washout experiments show that older FN (green) is translocated deep into the gland at the base of deepening clefts, whereas new FN (red) assembly occurs behind it. We propose that the dynamic inward translocation of FN as a wedge, followed by later assembly behind it, provides the missing mechanism for precise local deposition of FN synthesized by a broad zone of cells surrounding developing clefts. The local wedge of FN would mediate the previously described conversion of E-cadherin cell-cell adhesions to integrin-mediated cell-matrix adhesions, thereby promoting the separation of actively jostling cells to form the cleft during branching morphogenesis.

The purpose of the dynamic and relatively random cell movements during early development may be to provide adequate tissue plasticity for local remodeling by assembling fibronectin. Because such major cell rearrangements must occur in order to transform the aggregate of undifferentiated cells comprising the primary bud into a highly ordered system of ducts and acini later in development, it is not surprising that the cells are highly mobile. It is interesting that cell movements differ within subregions of the gland, and it is not surprising that bud (preacinar) cells are more migratory than duct cells, given that acini are more complex structures than ducts and maturation of ducts begins early in development at E14 (Hashizume and Hieda, 2005).

Another function of cell migration during early development may be to allow cells in the general vicinity of the cleft to participate in highly localized matrix assembly. We previously reported puzzling in situ hybridization findings, showing expression of FN mRNA by cells in the E12 SMG cleft region extending several cell diameters away from the cleft, even though FN was deposited only within the cleft and not at interior sites (Sakai et al., 2003). It was unclear why cells so far from the site of deposition should express FN. Here, we report that cells can – and do – migrate from interior regions of the bud to the basement membrane, where these cells may deposit FN. In fact, careful comparisons of the basement membrane with GFP-labeled cells revealed that, when cells contacted the basement membrane, there was often a focal increase in Alexa Fluor-647-FN intensity (M.L., unpublished observation), implying local FN assembly.

Cell migration has been implicated in branching morphogenesis in other cell culture models and other organs. Movements of GFP-labeled cells were observed in the tips of the ureteric bud (UB) and were described as ‘short-range’ movements (Shakya et al., 2005). Although these UB movements were not quantified, comparisons of the short-range cell movements in the tips of the buds with those in SMGs over the same time periods reveal that the UB cell movements are much less extensive than those occurring in the developing SMG. UB ductal cells were immobile, perhaps because these cells enclose a central lumen (Meyer et al., 2004). Migration is also implicated in branching morphogenesis of the mammary gland for invasion of the epithelium into the surrounding fat pad (Affolter et al., 2003). Similarly, the imaging of *Drosophila* trachea revealed dynamic filopodial cell extensions along the basal surface at the initiation of protrusions (Ribeiro et al., 2002). In contrast to the mammary gland and trachea, SMG epithelial cells do not show evidence of invasion through the basement membrane at early stages of branching morphogenesis; the cells remain confined within the basement-membrane barrier while undergoing dynamic rearrangements. Branching of the mammary gland and trachea might therefore be more similar to the in vitro process of tubulogenesis (Pollack et al., 2004; Pollack et al., 1998). The new mechanism we describe for salivary gland branching morphogenesis may be partially shared with other branching organs, such as kidney and pancreas.

However, in contrast to tubulogenesis, where tight junctions are maintained throughout branching, rapid losses of cell-cell contacts appear to occur as cells migrate apart in the SMG

during branching morphogenesis. This highly dynamic process suggests that the cells are connected by transient adhesion structures without mature epithelial junctional complexes. In fact, previous studies demonstrated the absence of mature adherens junctions and a progressive incorporation of E-cadherin into actin-containing adhesion structures relatively late in SMG development. Between E15 and E18, E-cadherin became progressively associated with the Triton X-100-insoluble actin cytoskeletal fraction rather than the soluble cytosolic fraction (Menko et al., 2002), suggesting increasing association with adherens junctions. Moreover, embryonic SMGs lack mature tight junctions. Even though tight junctions exist in the original oral epithelium from which the SMG originates, they are not found in the early embryonic SMG epithelium (Hieda et al., 1996). Consistent with that study, even though we detected low levels of the tight junction protein ZO-1 (Stevenson et al., 1986) in E12 epithelial rudiments by immunostaining, it was not organized into tight junctions (M.L., C.W. and K.M.Y., unpublished data). Taken together, these data support the idea that SMG epithelial cells undergo a transient de-differentiation during morphogenesis (O'Brien et al., 2002), and cell migration and plasticity during early salivary gland branching morphogenesis is associated with the lack of mature, adhesive cell-cell contacts.

We have used live imaging of GFP-labeled cells and fluorescently labeled FN to gain new insights into the process of branching morphogenesis. Many live imaging studies have used GFP as an inert cell tracker to study cell and tissue movements during development, including neural crest migration (Elena de Bellard and Bronner-Fraser, 2005), vascularization in embryonic zebrafish (Lawson and Weinstein, 2002), cell movements during dorsal closure in *Drosophila* (Wood and Jacinto, 2005) and branching morphogenesis (Davies, 2005; Shakya et al., 2005; Srinivas et al., 1999; Watanabe and Costantini, 2004). Our method of using adenovirus to deliver GFP to cells has the advantage that a subset of cells can be labeled within a few hours in any mouse strain. Future live-imaging experiments, in which individual cell populations are imaged simultaneously with other molecular markers, should lead to refined models of the dynamic process of branching morphogenesis.

Materials and Methods

SMG organ culture

Timed-pregnant female mice of out-bred strain ICR were obtained from Harlan. Submandibular salivary glands (SMGs) were harvested from mouse embryos at 12 or 13 days gestation (E12 or E13) or from mouse pups at postnatal day 1 (P1). Animal protocols were approved by the NIDCR Animal Care and Use Committee.

Whole SMGs were cultured as previously described (Hoffman et al., 2002) except that for imaging they were cultured submerged in glass-bottom culture dishes (MatTek) coated with FN. To prepare epithelial rudiments for imaging, mesenchyme was removed from E12 and E13 SMGs as reported previously (Larsen et al., 2003). P1 SMGs were subjected to the identical enzymatic treatment, which did not completely remove the P1 mesenchyme. For imaging, P1 SMGs were cut into fragments similar in size to E12 rudiments. Epithelial rudiments were labeled with GFP by incubation for 1 hour at room temperature in a solution containing a replication-deficient adenovirus, Adeno-X-EGFP (Ad-GFP, BD Biosciences), diluted in HBBS, 10% BSA at 1.2×10^5 infectious units (ifu)/μl. The optimal dilution for detection by confocal microscopy was empirically determined by serial dilution, and the multiplicity of infection (MOI) was estimated to be 2-5, depending on the size of the glands. Epithelial rudiments were transferred to three-well, glass-bottom culture dishes (P50G-1.5-3x14F) (MatTek) and immersed in 10 μl of Phenol Red-free, growth-factor-reduced Matrigel (Kleinman et al., 1986) (BD Biosciences) diluted 1:1 in Dulbecco's modified Eagle's medium (DMEM) with Nutrient mixture F12 (Ham) (DME/F12) without Phenol Red (Invitrogen). After 15 minutes at 37°C, a Nuclepore Track-Etch membrane (13 mm, 0.2 μm, Whatman) was placed on top of the Matrigel. Following another 15-minute incubation, the well was filled with 200 μl of growth medium: DME/F12, containing ascorbic acid (150 μg/ml), transferrin (50 μg/ml), penicillin (100 U/ml), streptomycin (100 μg/ml), 100 ng/ml fibroblast growth factor 7 (FGF7), and 20 ng/ml epidermal growth factor (EGF).

SMGs were treated with the cell proliferation inhibitor hydroxyurea (EMD Biosciences) at 0.5 mM, after determining optimal concentrations with a dilution series. After 24 hours of time-lapse imaging, SMGs and non-imaged SMGs were pulsed with the thymidine analog 5-bromodeoxyuridine (BrdU, Roche) for 2 hours.

Alexa Fluor-647-FN

Human plasma fibronectin (FN) was prepared as described previously (Akiyama, 1999) and coupled to Alexa Fluor-647 or Alexa Fluor-488 at 2 mg/ml following the manufacturer's directions after dialysis against PBS (Invitrogen). Alexa Fluor-647-labeled human plasma FN (Alexa Fluor-647-FN) was included in growth media from the beginning of the culture period at 0.04 μg/μl in experiments where indicated. In washout experiments, the medium containing Alexa Fluor-647-FN was removed at the time indicated and replaced with fresh medium without labeled FN. In pulse-chase experiments, Alexa Fluor-647-FN was added after washout of Alexa Fluor-488.

Microinjection

E13 SMGs were incubated overnight on Nuclepore filters. Ad-GFP (1.34×10^4) in medium containing 1% (w/v) Fast Green (Sigma) to visualize the injection site, was microinjected into an epithelial bud at 3500 hPa with 700 hPa compensation pressure for 0.5 milliseconds using a FemtoJet microinjector (Eppendorf) and custom tips (Humagen).

Immunostaining

Immunofluorescence staining was performed as previously described (Larsen et al., 2003) on SMGs fixed with 4% paraformaldehyde (PFA) or with 2% PFA for GFP-expressing SMGs. SMGs treated with BrdU were fixed in ice-cold ethanol pH 2. Antibodies were obtained from the following sources and used at the indicated dilutions: E-cadherin (ECCD-2, Zymed, 1:100), E-cadherin (DECMA, BD Transduction, 1:200), BrdU (Roche, 1:10), and GFP (Abcam, 1:400).

Conventional time-lapse microscopy and image processing

Conventional widefield time-lapse microscopy was performed as previously described using an Axiovert 100 microscope (Carl Zeiss) fitted with a CoolSNAP ES cooled CCD camera (Photometrics) (Larsen et al., 2003), and enclosed in an environmental chamber (Precision Plastics) heated to 37°C and containing 5% CO_2 in 95% air. Images were captured and assembled into QuickTime (QT) format movies using MetaMorph software, and movies were compressed using the Sorenson codec in Quick Time Pro to create movies in QT or MPEG format of a small size. The extensive compression to meet JCS guidelines for supplemental file sizes occasionally resulted in minor pixel artifacts. Higher-resolution movies can be obtained from the authors upon request.

Confocal time-lapse microscopy and image processing

Time-lapse microscopy was performed using a 510 LSM scan head mounted on a fully motorized Axiovert 200 microscope (Zeiss) enclosed in a XL environmental chamber (Zeiss) heated to 37°C with an Air-Therm heater controller (WPI) with an atmosphere of 5% CO_2 in 95% air. Confocal stacks of 6-9 images (7 μm thick) were acquired using a Plan Apo 20× 0.75 NA objective. Acquisition settings were optimized to obtain maximum resolution of whole explants while minimizing photodamage. The Zeiss Multi-Time macro was used to acquire image stacks every 6 or 10 minutes at multiple stage locations. To assemble movies, confocal images from a central point in the SMG were imported as TIFF files into MetaMorph software (Molecular Devices) and reassembled into image stacks. GFP images were adjusted for brightness and contrast and a median filter was applied. QT format movies were created using MetaMorph followed by compression in Quick Time Pro using the Sorenson or Cinepak codec.

Quantitative morphometric analysis

To calculate distances between cells, single confocal images were calibrated and converted to a binary image to select cells, and then cell centroids were automatically determined. Distances between centroids were measured. Average cell diameter was calculated by averaging length and width for 30 cells from three random calibrated confocal images of three E-cadherin-stained SMG and is expressed ± s.d. To calculate the mitotic labeling index, confocal images of BrdU staining were converted to a binary image and pixel density was measured. From calibrated DIC images, the cell perimeter was traced, and the 2D area of each gland was calculated. BrdU labeling index was expressed as a ratio of the pixel density divided by the 2D area. Measurements of FN translocation rate were calculated by measuring the net displacement between the first and last image and dividing by the elapsed time. MetaMorph software (Molecular Devices) was used for all morphometric analysis.

Cell tracking

Single GFP-labeled cells chosen randomly were manually tracked in unaltered confocal image stacks using Volocity 3.6.1 software (Improvision). Cells were selected using the wand thresholding tool, and the location and the shape of each cell were recorded at each time point. Each cell was tracked in the *X*, *Y* and *Z* planes for 3 hours (18 frames) or 5 hours (30 frames), depending on the experiment. After a cell divided, the track of one daughter cell was followed. Cells that could not be tracked for the full time period (3 or 5 hours) or that underwent necrosis were excluded. Cell tracks from a representative experiment were created by the software based on positional information and plotted as 3D rose plots with each track starting from the origin (0, 0, 0). Total distance traversed (T, path of cell track), displacement (D, distance between starting and ending point), velocity (T/*t*), and meandering index (D/T, where 1 equals a straight line) were calculated using a minimum of 15 cells per treatment averaged from 2-6 independent experiments using Prism software (Graph Pad), with the actual numbers indicated in figure legends. Statistical significance was determined using the Wilcoxon signed-rank test, with *P* values indicated in the figure legends.

The authors thank C. Galbraith for advice on confocal microscopy, M. Hoffman, J. Koblinski, L. Angerer, M. Gerdes and members of the laboratory for helpful discussions and critical reading of the manuscript, and H. Grant for proofreading. This work was partially supported by a postdoctoral Ruth L. Kirschstein National Research Service Award (NRSA) from NIH, NIDCR to M.L., a Howard Hughes Medical Institute (HHMI) training award to C.H.W., and research support from the Intramural Research Program of the NIH, NIDCR, to K.M.Y.

References

Affolter, M., Bellusci, S., Itoh, N., Shilo, B., Thiery, J. P. and Werb, Z. (2003). Tube or not tube: remodeling epithelial tissues by branching morphogenesis. *Dev. Cell* **4**, 11-18.

Akiyama, S. K. (1999). Purification of fibronectin. *Curr. Protocols Cell Biol.* 10.5.1-10.5.13.

Barcellos-Hoff, M. H., Aggeler, J., Ram, T. G. and Bissell, M. J. (1989). Functional differentiation and alveolar morphogenesis of primary mammary cultures on reconstituted basement membrane. *Development* **105**, 223-235.

Davies, J. A. (2005). Watching tubules glow and branch. *Curr. Opin. Genet. Dev.* **15**, 364-370.

Elena de Bellard, M. and Bronner-Fraser, M. (2005). Neural crest migration methods in the chicken embryo. *Methods Mol. Biol.* **294**, 247-267.

Grobstein, C. (1953). Inductive epitheliomesenchymal interaction in cultured organ rudiments of the mouse. *Science* **118**, 52-55.

Hashizume, A. and Hieda, Y. (2005). Hedgehog peptide promotes cell polarization and lumen formation in developing mouse submandibular gland. *Biochem. Biophys. Res. Commun.* **339**, 996-1000.

Hieda, Y., Iwai, K., Morita, T. and Nakanishi, Y. (1996). Mouse embryonic submandibular gland epithelium loses its tissue integrity during early branching morphogenesis. *Dev. Dyn.* **207**, 395-403.

Hoffman, M. P., Kidder, B. L., Steinberg, Z. L., Lakhani, S., Ho, S., Kleinman, H. K. and Larsen, M. (2002). Gene expression profiles of mouse submandibular gland development: FGFR1 regulates branching morphogenesis in vitro through BMP- and FGF-dependent mechanisms. *Development* **129**, 5767-5778.

Keller, R. (2002). Shaping the vertebrate body plan by polarized embryonic cell movements. *Science* **298**, 1950-1954.

Kleinman, H. K., McGarvey, M. L., Hassell, J. R., Star, V. L., Cannon, F. B., Laurie, G. W. and Martin, G. R. (1986). Basement membrane complexes with biological activity. *Biochemistry* **25**, 312-318.

Larsen, M., Hoffman, M. P., Sakai, T., Neibaur, J. C., Mitchell, J. M. and Yamada, K. M. (2003). Role of PI 3-kinase and PIP3 in submandibular gland branching morphogenesis. *Dev. Biol.* **255**, 178-191.

Lawson, N. D. and Weinstein, B. M. (2002). In vivo imaging of embryonic vascular development using transgenic zebrafish. *Dev. Biol.* **248**, 307-318.

Lecaudey, V. and Gilmour, D. (2006). Organizing moving groups during morphogenesis. *Curr. Opin. Cell Biol.* **18**, 102-107.

Menko, A. S., Zhang, L., Schiano, F., Kreidberg, J. A. and Kukuruzinska, M. A. (2002). Regulation of cadherin junctions during mouse submandibular gland development. *Dev. Dyn.* **224**, 321-333.

Meyer, T. N., Schwesinger, C., Bush, K. T., Stuart, R. O., Rose, D. W., Shah, M. M., Vaughn, D. A., Steer, D. L. and Nigam, S. K. (2004). Spatiotemporal regulation of morphogenetic molecules during in vitro branching of the isolated ureteric bud: toward a model of branching through budding in the developing kidney. *Dev. Biol.* **275**, 44-67.

Morita, K. and Nogawa, H. (1999). EGF-dependent lobule formation and FGF7-dependent stalk elongation in branching morphogenesis of mouse salivary epithelium in vitro. *Dev. Dyn.* **215**, 148-154.

Nakanishi, Y., Morita, T. and Nogawa, H. (1987). Cell proliferation is not required for the initiation of early cleft formation in mouse embryonic submandibular epithelium in vitro. *Development* **99**, 429-437.

O'Brien, L. E., Zegers, M. M. and Mostov, K. E. (2002). Opinion: building epithelial architecture: insights from three-dimensional culture models. *Nat. Rev. Mol. Cell Biol.* **3**, 531-537.

Pankov, R., Cukierman, E., Katz, B. Z., Matsumoto, K., Lin, D. C., Lin, S., Hahn, C. and Yamada, K. M. (2000). Integrin dynamics and matrix assembly: tensin-dependent translocation of $\alpha_5\beta_1$ integrins promotes early fibronectin fibrillogenesis. *J. Cell Biol.* **148**, 1075-1090.

Pollack, A. L., Runyan, R. B. and Mostov, K. E. (1998). Morphogenetic mechanisms of epithelial tubulogenesis: MDCK cell polarity is transiently rearranged without loss of cell-cell contact during scatter factor/hepatocyte growth factor-induced tubulogenesis. *Dev. Biol.* **204**, 64-79.

Pollack, A. L., Apodaca, G. and Mostov, K. E. (2004). Hepatocyte growth factor induces MDCK cell morphogenesis without causing loss of tight junction functional integrity. *Am. J. Physiol. Cell Physiol.* **286**, C482-C494.

Ribeiro, C., Ebner, A. and Affolter, M. (2002). In vivo imaging reveals different cellular functions for FGF and Dpp signaling in tracheal branching morphogenesis. *Dev. Cell* **2**, 677-683.

Ridley, A. J., Schwartz, M. A., Burridge, K., Firtel, R. A., Ginsberg, M. H., Borisy, G., Parsons, J. T. and Horwitz, A. R. (2003). Cell migration: integrating signals from front to back. *Science* **302**, 1704-1709.

Sakai, T., Larsen, M. and Yamada, K. M. (2003). Fibronectin requirement in branching morphogenesis. *Nature* **423**, 876-881.

Shakya, R., Watanabe, T. and Costantini, F. (2005). The role of GDNF/Ret signaling in ureteric bud cell fate and branching morphogenesis. *Dev. Cell* **8**, 65-74.

Srinivas, S., Goldberg, M. R., Watanabe, T., D'Agati, V., al-Awqati, Q. and Costantini, F. (1999). Expression of green fluorescent protein in the ureteric bud of transgenic mice: a new tool for the analysis of ureteric bud morphogenesis. *Dev. Genet.* **24**, 241-251.

Stevenson, B. R., Siliciano, J. D., Mooseker, M. S. and Goodenough, D. A. (1986). Identification of ZO-1: a high molecular weight polypeptide associated with the tight junction (zonula occludens) in a variety of epithelia. *J. Cell Biol.* **103**, 755-766.

Takeichi, M. (1991). Cadherin cell adhesion receptors as a morphogenetic regulator. *Science* **251**, 1451-1455.

Watanabe, T. and Costantini, F. (2004). Real-time analysis of ureteric bud branching morphogenesis in vitro. *Dev. Biol.* **271**, 98-108.

Wood, W. and Jacinto, A. (2005). Imaging cell movement during dorsal closure in Drosophila embryos. *Methods Mol. Biol.* **294**, 203-210.

Yamada, K. M. and Olden, K. (1978). Fibronectins–adhesive glycoproteins of cell surface and blood. *Nature* **275**, 179-184.